Applied Computational Electromagnetics Society

Express Journal

ACES

September 2016

Vol. 1 No. 9

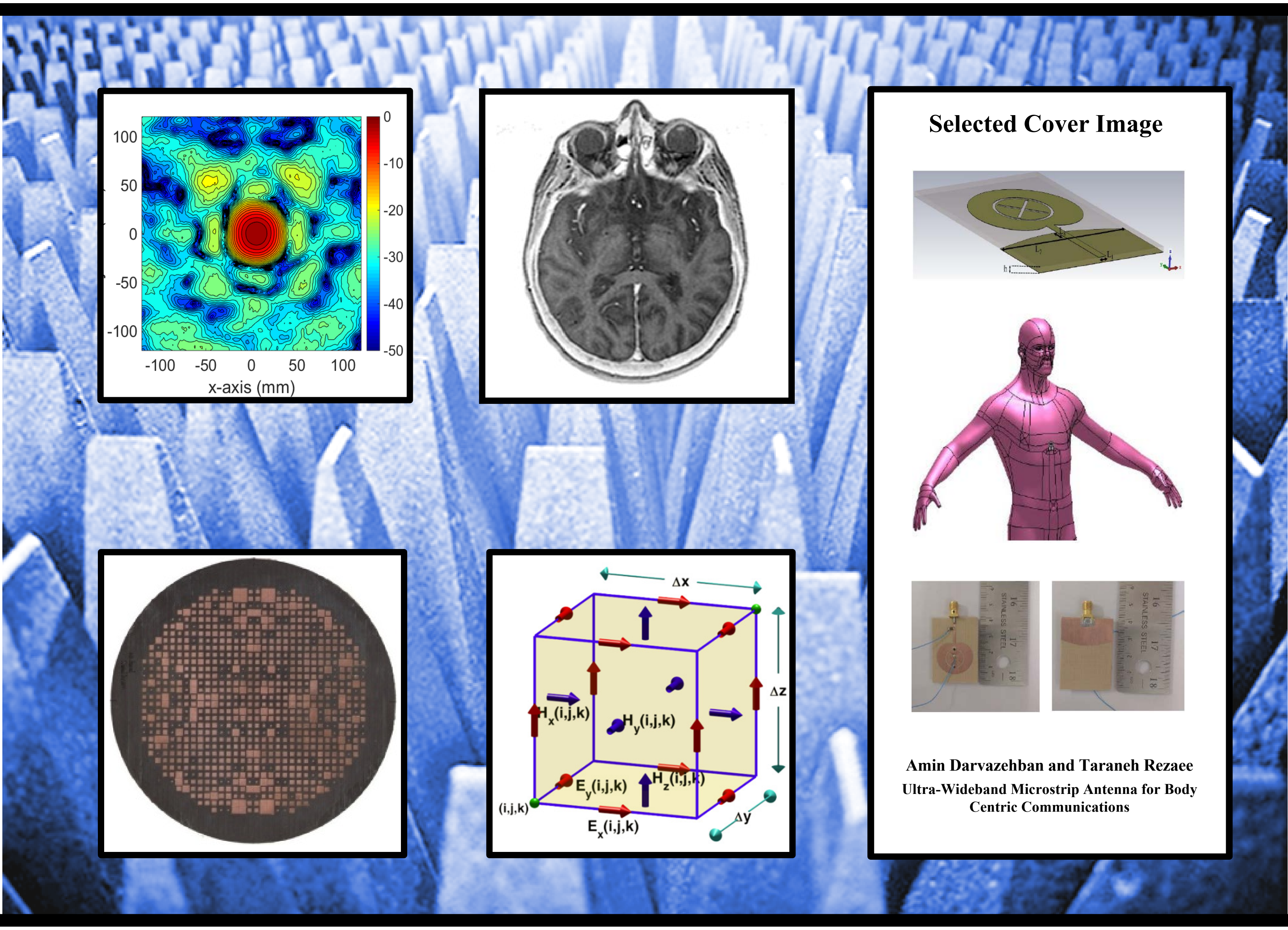

APPLIED COMPUTATIONAL ELECTROMAGNETICS SOCIETY EXPRESS JOURNAL

http://aces-society.org

GENERAL INFORMATION

PURPOSE AND SCOPE: The Applied Computational Electromagnetics Society ***(ACES) Express*** Journal hereinafter known as the ***ACES Express Journal*** is devoted to the timely and rapid exchange of information in computational electromagnetics, to the advancement of the state-of-the art, and the promotion of related technical activities. The primary objective of the information exchange is to inform the scientific community in a short amount of time on the developments of recent computational electromagnetics tools and their use in electrical engineering, physics, or related areas. The technical activities promoted by this publication include code validation, performance analysis, and input/output standardization; code or technique optimization and error minimization; innovations in solution technique or in data input/output; identification of new applications for electromagnetics modeling codes and techniques; integration of computational electromagnetics techniques with new computer architectures; and correlation of computational parameters with physical mechanisms.

SUBMISSIONS: The ***ACES Express Journal*** welcomes original, previously unpublished papers, relating to applied computational electromagnetics. Typical papers will represent the computational electromagnetics aspects of research in electrical engineering, physics, or related disciplines as well as research in the field of applied computational electromagnetics.

Manuscripts are to be submitted through the upload system of ***ACES*** web site http://aces-society.org Please see "Information for Authors" on inside of back cover and at ***ACES*** web site. For additional information contact the Editor-in-Chief:

Dr. Ozlem Kilic
Department of Electrical Engineering and Computer Science
The Catholic University of America
Washington, DC 20064
Email: kilic@cua.edu

SUBSCRIPTIONS: All members of the Applied Computational Electromagnetics Society are entitled to access and download the ***ACES Express Journal*** of any published journal article available at http://aces-society.org. ***ACES Express Journal*** is an online journal and printed copies are not available. Subscription to ACES is through the web site.

THE APPLIED COMPUTATIONAL ELECTROMAGNETICS SOCIETY EXPRESS JOURNAL

Vol. 1 No. 9 September 2016

TABLE OF CONTENTS

Capacitance Extraction for Microstrip Lines Using Conformal Technique Based on Finite-Difference Method

Yaxiu Sun and Xiaomeng Wang

College of Information and Communication Engineering
Harbin Engineering University, Harbin, 150001, China
sunyaxiu@hrbeu.edu.cn, wangxiaomeng@hrbeu.edu.cn

Abstract **─** In this paper, a novel method using conformal technique of finite-difference method (FDM) is proposed to capacitance extraction of microstrip lines. Instead of deriving the average dielectric constant ε, this method uses electric field numerical weights to process the inhomogeneous cells, and takes the discontinuous effects of both inhomogeneous Ampere cell and Faraday cell into account. Besides, a new boundary condition is proposed, where the cells obeying exponential distribution are added at boundary. The new method shows good agreement with the measurement and traditional methods.

Index Terms **─** Capacitance extraction, conformal technique, finite-difference method (FDM).

I. INTRODUCTION

Finte-difference method (FDM) has been widely used to solve variable electromagnetic problems, especially the extraction of distributed parameters [1-3]. When solving the capacitance parameter of microstrip lines, the cells divided from the electromagnetic space can be inhomogeneous, and the dielectric constants in one cell are not unique. Thus, the difference equations cannot be used directly. The general methods solving this problem are equivalent dielectric constant techniques [4-5]. They derive the average dielectric constants according to the relationships of cell loop's volume, area and length, but have neglected the inhomogeneous Faraday and Ampere cells. So a new conformal technique is proposed in this paper, which uses the electric field numerical weights to process inhomogeneous cells, and takes discontinuous effects of Ampere and Faraday cells into account.

Besides, when FDM is used to solve the open structures, boundary conditions are required to terminate the calculation space. Generally, there are two kinds of boundary conditions. One is absorbing boundary condition (ABC) according to the traveling wave equation [6], [7]. The other is perfectly matched layer (PML) based on the absorbing media [8]. ABC requires much less computation and memory than PML, but it may cause higher reflection and larger error. Hence, a new boundary condition is proposed, which cells obeying exponential distribution are added at the boundary. Finally, the proposed conformal technique and new boundary condition are verified by calculation.

II. FORMULATION

A. The iteration equation of FDM

The Gauss law can be represented as:

$$q = \oiint_s \boldsymbol{D} \cdot d\boldsymbol{s}\ , \tag{1}$$

where q is the total electric charge on the surface of the conductor, and $\boldsymbol{D}$ is the electric displacement vector which can be represented as $\boldsymbol{D}=\varepsilon\boldsymbol{E}$. Electric field intensity $\boldsymbol{E}$ can be represented by potential Φ as $\boldsymbol{E}=-\nabla\Phi$. The capacitance solving model is a dual regional structure whose dielectric constants are ε_1 and ε_2. So the spatial difference equations of $\boldsymbol{E}=-\nabla\Phi$ in these two regions can be described:

$$E_x[(i+\frac{1}{2})\Delta x, j\Delta y] = -\frac{\Phi[(i+1)\Delta x, j\Delta y]-\Phi(i\Delta x, j\Delta y)}{\Delta x}, \tag{2}$$

$$E_y[i\Delta x, (j+\frac{1}{2})\Delta y] = -\frac{\Phi[i\Delta x, (j+1)\Delta y]-\Phi(i\Delta x, j\Delta y)}{\Delta y}, \tag{3}$$

where i and j are any positive integers, Δx and Δy are the step size in x and y direction. So the divergence of electric displacement vector can be derived as:

$$\begin{aligned}&\nabla\cdot\boldsymbol{D}(i\Delta x, j\Delta y)\\ &= -\varepsilon_1\frac{\Phi[(i+1)\Delta x, j\Delta y]+\Phi[(i-1)\Delta x, j\Delta y]-2\Phi(i\Delta x, j\Delta y)}{(\Delta x)^2}\cdot\\ &-\varepsilon_2\frac{\Phi[i\Delta x,(j-1)\Delta y]-2\Phi[i\Delta x, j\Delta y]+\Phi[i\Delta x,(j+1)\Delta y]}{(\Delta y)^2}\end{aligned} \tag{4}$$

If $\varepsilon_1=\varepsilon_2$ and $\Delta x=\Delta y$, according to Laplace equation: $\nabla\cdot\boldsymbol{D}=0$, (4) can be simplified as follows:

$$\begin{aligned}\Phi(i\Delta x, j\Delta y) = \frac{1}{4}\{&\Phi[i\Delta x,(j+1)\Delta y]+\Phi[i\Delta x,(j-1)\Delta y]\\ &+\Phi[(i+1)\Delta x, j\Delta y]+\Phi[(i-1)\Delta x, j\Delta y]\}\end{aligned}. \tag{5}$$

Equation (1) can be finally updated as:

$$q = -\varepsilon\sum_{i=1}^{\infty}\sum_{j=1}^{\infty}\Phi(i\Delta x, j\Delta y)\ . \tag{6}$$

Submitted On: September 12, 2016
Accepted On: October 18, 2016

1054-4887

Equation (6) is the finite difference iteration equation to solve the capacitance, and the value of per unit length capacitance can be obtained from $C = q/V$.

B. The conformal technology based on FDM

Figure 1 shows the microstrip line model we analysis in this paper. Figure 1 (a) is the discrete grid model. Figure 1 (b) show the structure of microstrip line in Fig. 1 (a). All the simulation calculations in this paper are conducted on the basis of the model of Fig. 1 (b). As shown in Fig. 1 (a), each grid represents a cell. We can see that the dielectric constants of cells at the boundary between two regions cannot be unique. When using the new conformal technology to solve the inhomogeneous cells here, the process is divided into two parts: Faraday cell and Ampere cell.

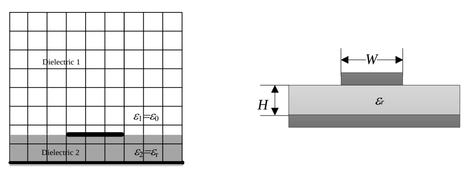

(a) (b)

Fig. 1. (a) The discrete grid model of microstrip line, and (b) structure of microstrip line with *W*/*H*=3, $\varepsilon_r = 4.4$.

As shown in Fig. 2, Faraday cell is divided into two regions with different dielectric constants ε_1 and ε_2 . Δx is divided into two parts: Δx_1 and Δx_2 . The electric field strengths of *x* and *y* direction are also divided into two parts: E_{x1} and E_{x2}, E_{y1} and E_{y2}. θ is the angle between *x* direction and interface.

The spatial derivative of Faraday's law can be written as:

$$
\begin{aligned}
&E_x^n(i+\frac{1}{2},j)\Delta x - E_x^n(i+\frac{1}{2},j+1)\Delta x + E_y^n(i,j+\frac{1}{2})\Delta y - E_y^n(i+1,j+\frac{1}{2})\Delta y \\
&= \mu\frac{1}{\Delta t}[H_z^{n+\frac{1}{2}}(i+\frac{1}{2},j+1) - H_z^{n+\frac{1}{2}}(i+\frac{1}{2},j+\frac{1}{2})]\Delta x\Delta y
\end{aligned}
\quad (7)
$$

According to electric field boundary conditions in perfect dielectric, the weights of dielectric 1 and dielectric 2 are defined as 1 and $\varepsilon_1/\varepsilon_2$ respectively. As shown in Fig. 3, E_{x1} and E_{x2} are discontinuous. Then electric field components can be weighted and the relationship after removing weights are:

$$
\begin{cases}
E_{x2} = E_{2N}\boldsymbol{e}_n + E_{2T}\boldsymbol{e}_t \\
E'_{2N} = \varepsilon_2 E_{2N}/\varepsilon_1 \\
E'_{2T} = E_{2T} \\
E'_{x2} = E'_{2N}\boldsymbol{e}_n + E'_{2T}\boldsymbol{e}_t
\end{cases}, \quad (8)
$$

where E'_{x2}, E'_{2N} and E'_{2T} are the weighted components. $\boldsymbol{e}_n$ and $\boldsymbol{e}_t$ are unit vectors.

To ensure the integration value unchanged, the weights of electric field components are taken into integral paths and the final update relationships are:

$$
\begin{cases}
\Delta N_2 = \Delta x_2 \sin\theta \\
\Delta T_2 = \Delta x_2 \cos\theta \\
\dfrac{\Delta N'_2}{\Delta N_2} = (\dfrac{E'_{2N}}{E_{2N}})^{-1} = \dfrac{\varepsilon_1}{\varepsilon_2}, \\
\dfrac{\Delta T'_2}{\Delta T_2} = (\dfrac{E'_{2T}}{E_{2T}})^{-1} \\
\Delta x'_2 = \sqrt{\Delta T'^2_2 + \Delta N'^2_2}
\end{cases} \quad (9)
$$

where ΔN_2 and ΔT_2 are the normal component and tangential component after orthogonal decomposition of Δx_2 , $\Delta N'_2$ and $\Delta T'_2$ are the component values of ΔN_2 and ΔT_2 after expanding or reducing. $\Delta x'_2$ is the total length after adjusting the path of field component. So the modified total length of the integral path can be obtained from (9):

$$
\Delta x' = \Delta x_1 + \Delta x'_2 = \Delta x_1 + \Delta x_2\sqrt{\cos^2\theta + \sin^2(\theta\frac{\varepsilon_1^2}{\varepsilon_2^2})} . \quad (10)
$$

So we use $\Delta x'$ instead of Δx to calculate (7).

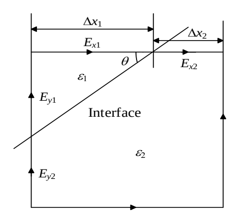

Fig. 2. The inhomogeneous Faraday cell model.

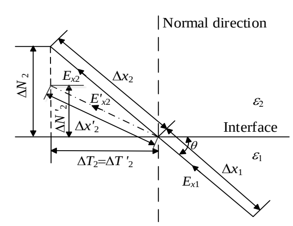

Fig. 3. The conformal process for Faraday loop path.

The conformal process of Ampere cell is same to the Faraday cell, and the Ampere cell model is shown in Fig. 4. The spatial derivative of Ampere's law can be written as:

$$
H_z^{n-\frac{1}{2}}(i+\frac{1}{2},j+\frac{1}{2}) - H_z^{n-\frac{1}{2}}(i+\frac{1}{2},j-\frac{1}{2}) = \Delta y(\frac{\partial D_X}{\partial t})^n_{(i+1/2,j)} ,(11)
$$

Δy is the total length of Ampere loop integral path.

According to electric displacement vectors boundary conditions in perfect dielectric, the weights of two kinds of media can be defined as 1 and $\varepsilon_2/\varepsilon_1$. The positional relationships are shown in Fig. 5. So the relationship between the components after removing the weights can be written as:

$$\begin{cases} D'_{2N} = D_{2N} \\ D'_{2T} = D_{2T}\,\varepsilon_1/\varepsilon_2 \end{cases}, \tag{12}$$

where D'_{2N} and D'_{2T} are the weighted components. Then taking the weights into the integral path:

$$\begin{cases} \Delta T_2 = \Delta y_2 \cos\varphi \\ \Delta N_2 = \Delta y_2 \sin\varphi \\ \dfrac{\Delta N'_2}{\Delta N_2} = \left(\dfrac{D'_{2T}}{D_{2T}}\right)^{-1} = \dfrac{\varepsilon_2}{\varepsilon_1} \\ \dfrac{\Delta T'_2}{\Delta T_2} = \left(\dfrac{D'_{2N}}{D_{2N}}\right)^{-1} \\ \Delta y'_2 = \sqrt{\Delta N'^2_2 + \Delta T'^2_2} \end{cases}, \tag{13}$$

where ΔN_2 and ΔT_2 are the initial length of normal and tangential component, which are obtained from orthogonal decomposition Δy_2, $\Delta y'_2$. $\Delta N'_2$ and $\Delta T'_2$ are the length after adjusting the path of field component. So the modified total length of the integral path is:

$$\Delta y' = \Delta y_1 + \Delta y'_2 = \Delta y_1 + \Delta y_2 \sqrt{\cos^2\phi + \sin^2\phi \frac{\varepsilon_1^2}{\varepsilon_2^2}}\ . \tag{14}$$

So we use $\Delta y'$ instead of Δy to calculate (11).

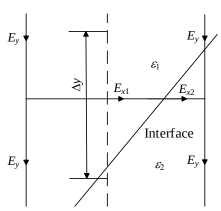

Fig. 4. The inhomogeneous Ampere cell model.

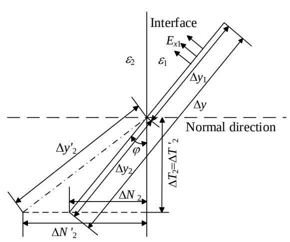

Fig. 5. The conformal process for Ampere loop path.

After above process, ε_2 and ε_1 has been converted as ε_e. So the relationship between electric field strength and electric displacement can be expressed by $\boldsymbol{D} = \varepsilon_e \boldsymbol{E}$.

C. A new boundary condition

A new boundary condition is proposed in the paper, which cells obeying exponential distribution are added at the boundary. Taking *x* direction for example, the electric field distribution obeys e^{-kx}, where *k* is a positive number. The outermost cells are considered infinitely long. When *x* tends to infinity, e^{-kx} is close to zero. So the outermost cells are described and the potentials are zero at infinity points.

III. NUMERICAL RESULTS

To verify the validity of new boundary condition, we use the mesh Δx=Δy=10^{-3}m to calculate the region where the coordinate is $x\in$[-39Δx, 39Δy] and $y\in$[-39Δx, 39Δy]. The potential at infinity is set at 0. We add the conductors with +10V at (-20Δx, -20Δy) and -10V at (20Δx, 20Δy) respectively.

Now the electric field distributions using different boundary conditions are shown in Fig. 6 and Fig. 7. One is the traditional boundary condition which is similar to a rectangle shield and the potential is $\Phi = 0$. The other is the new boundary condition in this paper. The electric field strength shown in Fig. 6 attenuates slowly in the diagonal direction. Whereas the electric field strength shown in Fig. 7 is closer to the potential distribution model with the same amount unlike charges. So the new boundary condition proposed in this paper is more applicable to solve the capacitance.

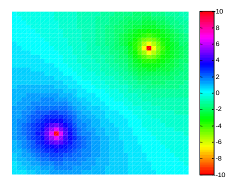

Fig. 6. The electric field distribution under traditional boundary condition.

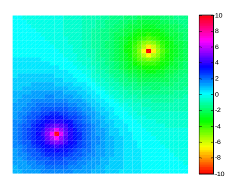

Fig. 7. The electric field distribution under new boundary condition.

Now the new method using conformal technique and new boundary condition has been applied to calculate the capacitance of microstrip line in Fig. 1. There are 79×79 grids in simulation area, and we use the mesh Δx=Δy=10^{-3}m to calculate the region where the coordinate is $x\in$[-39Δx, 39Δy] and $y\in$[-39Δx, 39Δy]. The potential at infinity is set at 0. The potential of microstrip line at [-39Δx≤x≤39Δx, -39Δy≤y≤-38Δy] is +10V, and the potential of microstrip line at [-6Δx≤x≤6Δx, -35Δy≤y≤-34Δy] is -10V. The dielectric constant is ε_r=4.4, which is distributed in the area of [-39Δx≤x≤39Δx, -38Δy≤y≤-35Δy].

Figure 8 and Fig. 9 show the potential distributions of Fig. 1 under the new boundary. Whereas the Fig. 9 has used the conformal technique and Fig. 8 has not. The scattered field at the cross media shown in Fig. 9 is more obvious than in Fig. 8. Moreover, the per unit length capacitance obtained from Fig. 8 is 101.47pF/m, and the value obtained from Fig. 9 is 97.759pF/m. Furthermore, the per unit length capacitance has been measured by the static field capacitance measurement method. It uses galvanometer measured the charge of microstrip line in case of a given voltage. Then the per unit length capacitance can be obtained and the value is 97.761pF/m. So the value of capacitance is closer to the measurement when using new conformal technology.

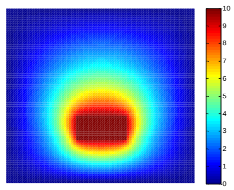

Fig. 8. The potential distribution without using conformal technique.

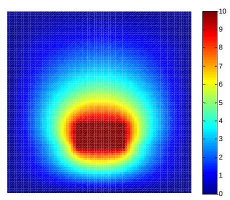

Fig. 9. The potential distribution using conformal technology.

Besides, to verify the accuracy of new method further, the average dielectric constant method has been used to calculate the capacitance of the microstip line model in Fig. 1 (b), and the discrete grid model is shown in Fig. 10. The potential distribution using the average dielectric constant method is shown in Fig. 11, and the per unit length capacitance is 96.87pF/m. The comparative result shows that the capacitance calculated by the new method is more approximated to the measurement than the average dielectric constant method. It shows that the new method has higher precision than the average dielectric constant method.

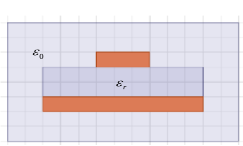

Fig. 10. The microstrip line model using average dielectric constant method.

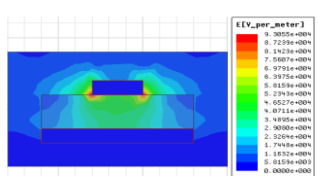

Fig. 11. The potential distribution of Fig. 10 model.

IV. CONCLUSION

A new method based on FDM has been proposed for capacitance extraction of microstrip line using conformal technique. The results show that the capacitance solved by the proposed method is close to the measurement and more accurate than traditional one. Besides, the new method can be applied to various positional relationships between dielectric interface and electric field directions. It also has a significance to the analysis and design of high speed PCB.

ACKNOWLEDGMENT

This project was supported by the National Natural Science Foundation of China (Grant No. 51209055), the China Postdoctoral Special Foundation (Grant No. 2015T80324), and the Natural Science Foundation of Heilongjiang, China (Grant No. F2015028).

REFERENCES

[1] Y. Liu, K. Lan, and K. Mei, "Capacitance extraction for electro static multiconductor problems by on-surface MEI," *IEEE Trans. Advanc. Packag.*, vol. 23, no. 3, pp. 489-494, 2000.

[2] J. Wang, W. Y. Yin, and Q. H, Liu, "FDTD (2, 4)-compatible conformal technique for treatment of dielectric surfaces," *Electronics Lett.*, vol. 45, no. 3, pp. 146-147, Jan. 29, 2009.

[3] J. Wang, W. Y. Yin, and Y. S. Xia, "A novel conformal surface current technique for large problems based on high-performance parallel FDTD method," *IEEE Antennas and Wireless Propag. Lett.*, vol. 12, pp. 11-14, 2013.

[4] L. Liou, Y. Mah, and A. Ferendeci, "Equivalent circuit parameter extraction of microstrip coupling lines using FDTD method," *IEEE Int. Symp. Antennas Propag.*, vol. 3, pp. 2488-1491, 2000.

[5] W. Yu and R. Mittra, "A conformal finite difference time domain technique for modeling curved dielectric surfaces," *IEEE Microw. Wireless Comp. Lett.*, vol. 11, no. 1, pp. 25-27, Jan. 2001.

[6] J. Zhou and J. Zhao, "Efficient high-order absorbing boundary conditions for the ADI-FDTD method," *IEEE Microw. Wireless Comp. Lett.*, vol. 19, no. 1, pp. 25-27, Jan. 2009.

[7] H. Shao, W. Hong, and Y. Zhou, "Generalized Z-domain absorbing boundary conditions for the analysis of electromagnetic problems with finite-difference time-domain method," *IEEE Trans. Microw. Theory Tech.*, vol. 51, pp. 82-90, 2003.

[8] S. Wang and F. L. Teixeira, "An efficient PML implementation for the ADI-FDTD method," *IEEE Mirow. Wireless Compon. Lett.*, vol. 13, no. 2, pp. 72-74, Feb. 2003.

Ultra-Wideband Microstrip Antenna for Body Centric Communications

Amin Darvazehban [1] and Taraneh Rezaee [2]

[1] Department of Computer and Electrical Engineering
Amirkabir University of Technology, Tehran, Iran
Amin.darvazehban@gmail.com

[2] Department of Biomedical Engineering
Islamic Azad University, Tehran, Iran
Taraneh.rezaii@yahoo.com

Abstract **─** A novel low profile reconfigurable wide band microstrip antenna for impulse radio ultra-wideband (IR-UWB) WBANs and targeted for on-body sensor node has been introduced. The printed monopole antenna consists of a heart shaped radiating patch and an elliptical ground plane. This antenna has a frequency bandwidth of 130% with a VSWR of 1.5 and average gain is about 3.6 dBi. There is a slot on the patch which is loaded by two varactor diodes to form a tunable notch band. The antenna operates from 2.4 GHz to 12 GHz. The proposed antenna is a good candidate for medical purpose since it has a sufficient amount of gain and bandwidth. We used active circuit to increase the flexibility of setting rejection band to prevent having interference from other sources such as Wi-Fi. The antenna is fabricated and there is a good agreement between the simulation and measurement results.

Index Terms **─** Body-centric wireless communication, miniaturized microstrip antenna, wireless body networks.

I. INTRODUCTION

Antenna designing for WBAN system is challenging due to the human body effect. Especially, providing the sufficient gain and efficiency of an antenna is the main issue of on-body to on-body communication. To overcome this problem, an on-body antenna should have vertical polarization relative to the human body surface. In addition, to satisfy the propagation along the body surface for on-body to on-body communication, the antenna is required to have omnidirectional radiation characteristic [1]. Also, a number of techniques aimed at minimizing the cost of such antenna without significantly sacrificing performance have been considered. One of the most important techniques is using slots on the patch surface. Slots perturb antenna current on the antenna surface and increase antenna bandwidth [2]. Another advantage of using slots is changing antenna polarization or using as a Frequency Selective Surface (FSS) to filter unwanted frequencies [3]. In some paper, small slots are imbedded on ground plane or feeding point to have better matching response. These techniques are well-known as Defected Ground Structure (DGS) and Defected Microstrip Structure (DMS) [4]. PIN diodes have been also used to change the antenna dimensions electrically and increase the frequency bandwidth [5]. In this paper, we use varactor diodes to increase the frequency bandwidth. The varactor diode is a variable capacitor which can be modelled as a series capacitor and a resistor to model the ohmic losses [6, 7]. To improve frequency and pattern bandwidth, heart-shaped printed monopole antenna is proposed in [8]. In this paper, a low profile ultra-wideband on-body antenna is presented. The proposed antenna has a low profile, omnidirectional radiation patterns in the whole UWB band, and maximum radiation along the near body surface. We also use antenna with slot and taper heart-shaped to increase frequency bandwidth. In some purposes we need filter to cut the frequency bandwidth, two varactor diodes are used to change the notch in frequency bandwidth. When we change the DC bias of the diodes, their capacitance values change. So this antenna is combination of filter and antenna. The proposed low profile UWB antenna is suitable for on-body communications since the field is vertically polarized and propagated along the body surface for IEEE 802.11b/g and IEEE 802.11a. The antenna is considered to operate as a relay between sensors located on the body and non-local station so it is an advantage for the antenna to be able to have tangential radiation over the body surface in the on-body mode and a bore sight pattern in the off-body mode at the frequency bands of 802.11a and 802.11b/g, respectively [9, 10]. This antenna has a frequency bandwidth of 130% with a VSWR of 1.5, average gain is about 3.6 dBi.

II. DESIGN OF A SLOTTED MICROSTRIP ANTENNA

As it is shown in Fig. 1, the proposed slot antenna

Submitted On: September 14, 2016
Accepted On: December 26, 2016

with line feed has been designed on Rogers RO4003 with permittivity of ε_r=3.2 and substrate thickness of h=0.813 mm and substrate size of 42×30 mm. The dimensions of slots and antenna are mentioned in Table 1.

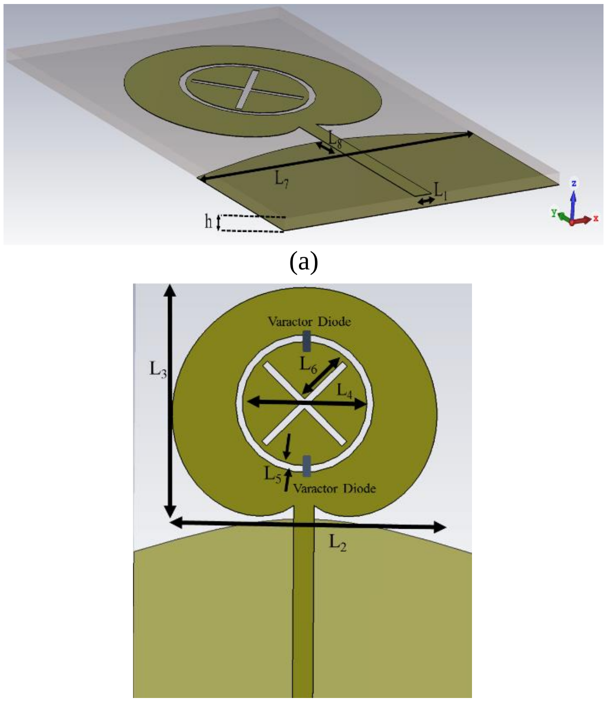

(a)

(b)

Fig. 1. Proposed slotted microstrip antenna: (a) side view, and (b) top view.

Table 1: Physical dimension of loaded-monopole

Parameter	L_1	L_2	L_3	L_4	L_5
Dimension (mm)	1.8	22	20	10	0.5
Parameter	L_6	L_7	L_8	h	
Dimension (mm)	4.7	30	2.3	0.813	

Two varactor diodes are used to change the capacitance value of the circular slots and these slots create notch in the frequency band. The notch band avoid interference with other frequency bands. Circular slots create notch in the frequency band. Line feed should be adjusted for 50Ω transmission line [11].

To increase the frequency bandwidth, two crossed slots are designed on the surface of the microstrip patch. These slots decrease antenna patch area and based on the following formula, quality factor of the microstrip antenna decreases. S is the area of the patch and f_r is the resonant frequency of the microstrip antenna. Frequency shift for patch is given as [12]:

$$\left|\frac{\Delta S}{S}\right| = \frac{1}{Q_0}\,, \tag{1}$$

$$\Delta f_1 = f_{0r}/2Q_0\,. \tag{2}$$

III. RESULTS AND DISCUSSION

With the dimensions given in Table 1, the proposed antenna was simulated in close proximity of the human body. To obtain the human effect on the antenna behavior, VOXEL model of body with CST software is simulated. The human body model was developed in the CST microwave studio. It is an adult male of mass 100 kg, height 180 cm and chest circumference of 115 cm, including muscle, skeleton and brain with human tissue. The electrical properties were defined at the frequency band of 2.5-12 GHz with resolution of 100 MHz. Figure 2 shows the placement of the antennas on the model. The antenna is placed 2 mm apart from the chest of the model. The on body simulated and measured S_{11} of the proposed antenna are illustrated in Fig. 3 and Fig. 5. As shown in Fig. 3, the bandwidth of the antenna can be changed from 2.5 GHz to 12 GHz in transmitting purposes and 2 GHz to 12 GHz in receiving purposes. As it is shown in Fig. 6, the human body behaves like a reflector and improves gain of the antenna because the permittivity of the body is about 42. The backlobe part of the antenna pattern is removed. In these types of antennas each part of the antenna has different resonant frequency, therefore the impedance bandwidth is wider than typical microstrip antenna. To obtain better results all dimensions are optimized. We have used Particle Swarm Algorithm with CST software. It is observed that the variation in the diameter of the metallic arcs has major effect on the lower frequency bandwidth. In case of impedance bandwidth, it improves return loss at higher frequency region and does not affect the lower cut-off frequency. The simulated antenna VSWR referenced to 50Ω is shown in Fig. 4. The improvement in the input impedance bandwidth using slots and curved ground plane is clear. It is interesting to mention that at low frequencies, the input impedance of the antenna is depended on the patch dimensions not the substrate dimensions.

At high frequencies the input impedance is intensively affected by the substrate thickness. We can improve matching parameter using elliptical ground plane. It is obvious that the radiation patterns changes slightly at higher frequency because of variation antenna dimensions at different frequencies. It means that radiation pattern bandwidth is smaller than impedance bandwidth. In portable system, this is negligible since we do not have constant and stable direction for transmitter. This antenna is so small and can be used in medical purposes. For example, in some frequencies such as Wi-Fi, interference is inevitable and we need an antenna that can filter unwanted frequencies. These diodes are used for creating notch to reject these frequencies. In this paper we used tapered elliptical form for the structure to get better impedance matching. The radiation patterns of the antenna when the antenna is attached to the body are changed. The body behaves like a reflector because the body permittivity ε_r=42 is so high. To verify the simulation result, the antenna has been fabricated and tested (see Fig. 7).

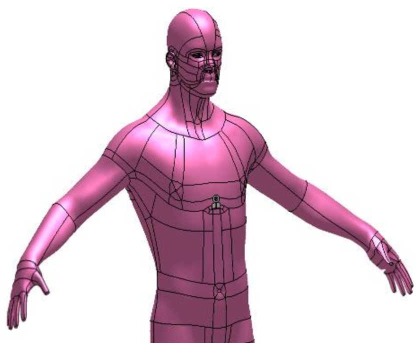

(a) Remote view

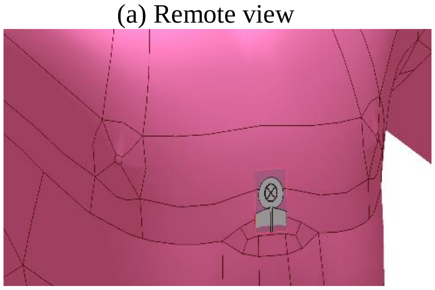

(b) Close view

Fig. 2. The proposed antenna placed on the chest human body model.

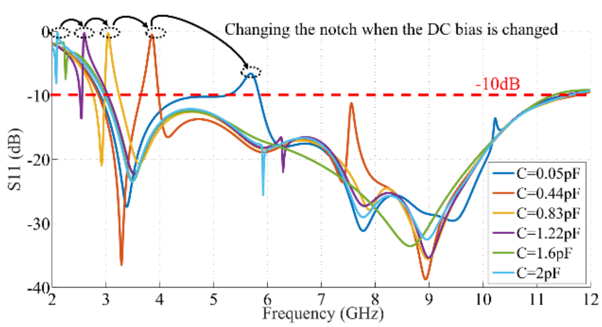

Fig. 3. Simulated S_{11} with CST software for different capacitance values on body.

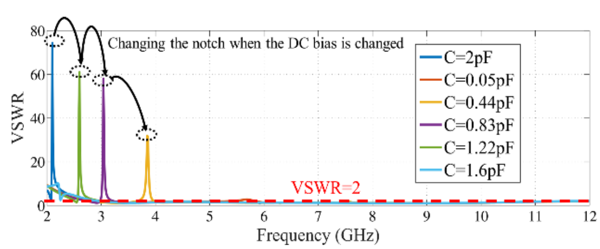

Fig. 4. VSWR of the slotted microstrip antenna.

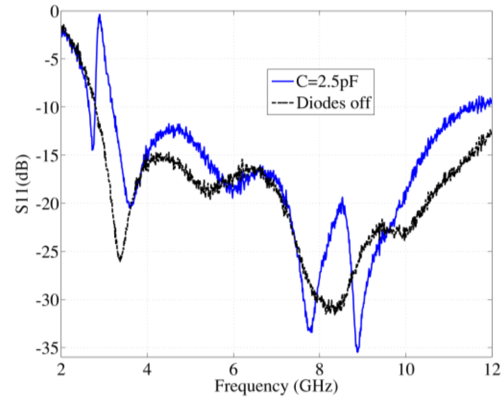

Fig. 5. Measured S_{11} in two states: 1-Diodes ON, 2-Diodes OFF.

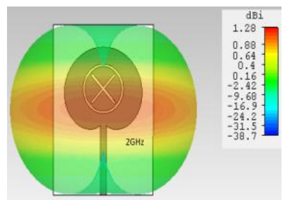

f=2 GHz, Gain=1.28 dB

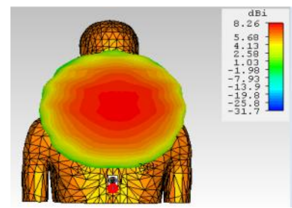

f=2 GHz, Gain=8.26 dB

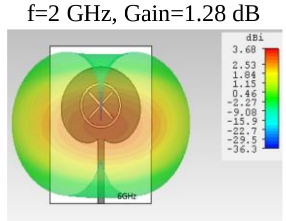

f=6 GHz, Gain=3.68 dB

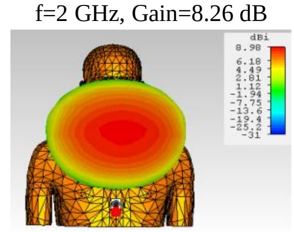

f=6 GHz, Gain=8.98 dB

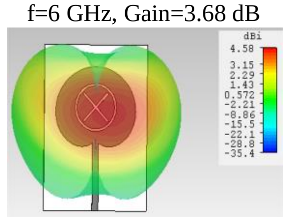

f=12 GHz,Gain=4.58 dB

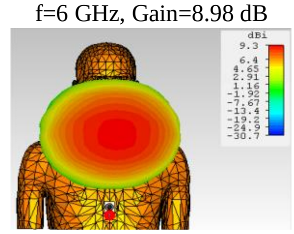

f=12 GHz, Gain=9.3 dB

Fig. 6. Comparision of the antenna radiation patterns at different frequencies with human body and without human body.

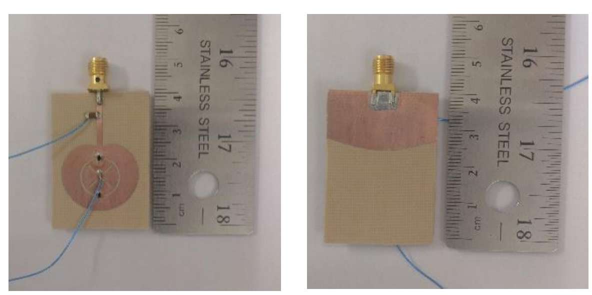

Fig. 7. Photo of fabrication.

VI. CONCLUSION

An efficient wide band and dual pattern heart-patch antenna with two varactor diodes and strip line feed is proposed for on-body and off-body communication modes is proposed and analysed with respect to the bandwidth, average gain, radiation pattern. The impedance bandwidth of proposed antenna achieved 130% from frequency range 2.8 to 12 GHz. The average gain of the antenna is about 3.5 dBi. The radiation pattern of E- plane & also studied. It has Bi-directional E-plane & Omni-directional H-plane. This antenna is simple in structure and easy to fabricate with MIC/MMIC systems. This antenna can be used for wireless communication systems, especially for medical purposes. We can adjust notch frequency band of the antenna easily by changing DC bias of the varactor diodes. The proposed antenna presents much improved gain with one tapered shape radiating element than the previous works of the compact dual band and dual mode antennas. The results show that this antenna does not experience significant frequency detuning from the free space resonance at whole frequency bands when simulated on the human body.

REFERENCES

[1] G. A. Conway and W. G. Scanlon, "Antennas for over body-surface communication at 2.45 GHz," in *Antennas and Propagation, IEEE Transactions on*, vol. 57, no. 4, pp. 844-855, Apr. 2009.

[2] K. M. Chang, R. J. Lin, I. C. Deng, J. B. Chen, K. Q. Xiang, and C. J. Rong, "A novel design of a CPW-fed square slot antenna with broadband circular polarization," *Microwave. Opt. Technol. Lett*., vol. 48, no. 12, pp. 2456-2459, Dec. 2006.

[3] O. Manoochehri, S. Abbasiniazare, A. Torabi, and K. Forooraghi, "A second-order BPF using a miniaturized-element frequency selective surface," *Progress In Electromagnetics Research C*, vol. 31, pp. 229-240, 2012.

[4] M. A. Salari, O. Manoochehri, and S. Abbasiniazare, "Miniaturized microstrip ring hybrid with defected microstrip structure," *Microwave and Optical Technology Letters*, vol. 55, pp. 2245-2248, 2013.

[5] S. Abbasiniazare, O. Manoochehri, and K. Forooraghi, "A reconfigurable printed dipole antenna using RF PIN diodes," *Microwave and Optical Technology Letters*, vol. 56, pp. 1151-1155, 2014.

[6] M. Noroozіarab, Z. Atlasbaf, M. Rafaei-Booket, and F. Farzami, "A tunable transmission line based on an SIW loaded by a new single-cell meta-material," *Telecommunications (IST), 2012 Sixth International Symposium on*, Tehran, pp. 75-79, 2012.

[7] F. Farzami and M. Norooziarab, "Experimental realization of tunable transmission lines based on single-layer SIWs loaded by embedded SRRs," in *IEEE Transactions on Microwave Theory and Techniques*, vol. 61, no. 8, pp. 2848-2857, Aug. 2013.

[8] C. Hua, Y. Lu, and T. Liu, "Printed UWB heart-shaped monopole antenna with band-notch reconfigurability," in *2016 IEEE International Workshop on Electromagnetics: Applications and Student Innovation Competition (iWEM)*, pp. 1-3, 2016.

[9] G. A. Conway, W. G. Scanlon, and D. Linton, "Low profile microstrip patch antenna for over-body surface communication at 2.45 GHz," in *Vehicular Technology Conference, 2007, VTC2007-Spring, IEEE 65th*, pp. 392-396, Apr. 22-25, 2007.

[10] S. Khaledian and Z. Atlasbaf, "Dual band and dual mode microstrip antenna for body centric wireless communication," *Applied Computational Electro-magnetics Society Journal*, vol. 31, 2016.

[11] I. J. Bahl and R. Garg, "A designer's guide to stripline circuits," *Microwaves*, pp. 90-96, Jan. 1978.

[12] J. R. James, et al., *Microstrip Antenna Theory and Design*. Steven-age, UK: Peter Peregrinus, 1981.

A Simple Analytical Method to Calculate Bending Loss in Dielectric Rectangular Waveguides

Kim Ho Yeap, Andrew Wei Chuen Tan, Koon Chun Lai, and Humaira Nisar

Faculty of Engineering and Green Technology
Tunku Abdul Rahman University, Kampar, Perak, 31900, Malaysia
yeapkh@utar.edu.my, evilfire8laster@1utar.my, laikc@utar.edu.my, humaira@utar.edu.my

Abstract **─** We present a simple analytical method to compute attenuation in bent dielectric rectangular waveguides. An approximate formulation for the attenuation constant is first derived by determining the ratio of average power loss per unit length to the average power propagating along the waveguide. Since the waveguide has been simplified into a slab in the process of derivation, losses at the four edges of the structure have been neglected. To account for these losses, the perturbation theory has been employed. The total loss is found to agree closely with that obtained via the Finite Element Method (FEM). Unlike the FEM which requires considerable computational time and power to solve, we demonstrate that the analytical method proposed here can easily be applied and it gives sufficiently accurate result.

Index Terms **─** Analytical method, attenuation constant, bending loss, perturbation theory, propagation constant, rectangular waveguides.

I. INTRODUCTION

Dielectric waveguides, such as optical fibers, have been widely used in the fields of telecommunication and integrated optics to channel signal from one end to another. In a dielectric waveguide, the core dielectric rod is immersed in one or more layers of dielectric materials which are of lower index of refraction n_2 than the core material itself n_1. This allows wave to propagate in the waveguide based on the principle of total internal reflection, described by Snell's law [1, 2]. In order to ensure that the information carried by the modulating signal is preserved, it is important to minimize losses in the waveguide during wave propagation. The losses in a dielectric waveguide can generally be classified into dielectric loss and radiation loss. In a uniformly straight waveguide, the fields are mostly confined within the core of the waveguide. Hence, radiation loss is practically negligible in the waveguide. When certain curvatures occur in the waveguide, however, wave with angles of incident exceeding the critical angle tend to radiate out from the guiding structure [3]. Because of this reason, radiation loss or more commonly known as bending loss, in this case, can no longer be ignored. Since bent structures are inevitable when channeling the signal, both dielectric and bending losses are equally important when estimating the total loss in the waveguide. Developing mathematical expression to describe the presence of curvatures in a rectangular waveguide is inherently difficult. This is because a combination of Cartesian and cylindrical coordinates is required so as to define the cross section and the bending radius of the waveguide. Hence, analytical methods, found in most literatures [4-7], focus only on the analyses of uniformly straight waveguides. As can be seen from some of the recent literatures [8-11], computational methods such as Finite Domain Time Difference (FDTD) or Finite Element Method (FEM) are preferred when bending loss is to be accounted for in the calculation of loss. The algorithms used in computational methods discretize the solution space into meshes. The electric field in each mesh is then numerically calculated. Hence, although they produce accurate results, these methods typically consume substantial computational time and power. This is particularly true when fields are to be solved for signals with very small wavelength (such as THz or optical signal) propagating in a three dimensional structure where the number of meshes is exceptionally huge. Analytical methods, on the other hand, are simpler and require relatively less time and power to solve.

Marcatili [3] and Marcuse [12] were among some of the early researchers who had developed analytical solutions for bent rectangular waveguides. In the process of derivation, however, both of them had assumed the fields' radiation at the four corner regions of the waveguide to be negligible. Due to this reason, the loss found using their methods has been underestimated. It is worthwhile noting that, Marcatili's method is only valid when the wave is weakly guided (i.e., the difference between n_1 and n_2 is small), while Marcuse's method is not bounded by this limitation. Hence, Marcuse's method has the advantage of being applied in structures with arbitrary ratio of indices of refraction. In this paper, we present an improvement on the accuracy of

Submitted On: October 10, 2016
Accepted On: December 4, 2016

Marcuse's method. We consider a dielectric rectangular waveguide surrounded by homogeneous dielectric material in our study. In order to account for the loss at the corner regions, we incorporate into the formulation the correction factor developed by Deck et al. [13]. This paper shall be presented in such a way that, casual readers could appreciate the final mathematical expressions, without the need of going through the underlying mathematics.

II. FORMULATION

Figure 1 depicts the structure of a bent rectangular waveguide with width a and height b. When deriving the attenuation constant of the waveguide, Marcuse has first assumed the fields at the vicinity of a bent waveguide to be similar to that of a straight guide. The assumption should hold valid as long as the radius of curvature R is sufficiently large. When deriving the fields' expressions, he has also assumed that there is no field variation in the y direction. This allows the propagating waves to be described as simple TE and TM waves [12]. According to the law of conservation of energy, the rate of decrease of power is to be equivalent to the power loss. Hence, power loss Λ can be expressed as the ratio of average power loss per unit length Δp to the average power propagating along the waveguide p, i.e., [1, 12]:

$$\Lambda = \frac{\Delta p}{p}. \tag{1}$$

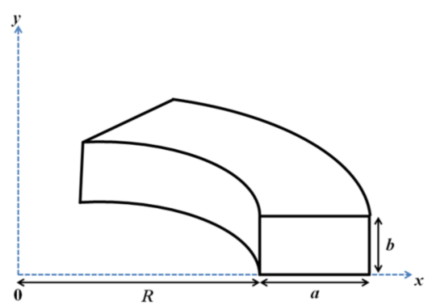

Fig. 1. A bent rectangular waveguide.

By substituting the fields' expression into (1), the loss equation Λ can be obtained as follows [12]:

$$\Lambda = \mathrm{Im}\left| \frac{2\sqrt{k_z^2 - n_2^2 k_2^2}\left(n_1^2 k_2^2 - k_z^2\right)}{k_2^2 k_z \left(n_1^2 - n_2^2\right)} \times \frac{\exp\left[a\sqrt{k_z^2 - n_2^2 k_2^2} - \frac{2\left(k_z^2 - n_2^2 k_2^2\right)^{1.5}(R + 0.5a)}{3k_z^2}\right]}{\left[a + \frac{1}{\sqrt{k_z^2 - n_2^2 k_2^2}} + \frac{1}{\sqrt{k_z^2 - n_1^2 k_2^2}}\right]} \right|, \tag{2}$$

where k_2 is the wavenumber of the dielectric cladding material and k_z is the propagation constant, which can be adopted from that of a straight waveguide. It is to be noted that k_z is a complex variable which comprises a phase constant β_z and an attenuation constant α_z, i.e., $k_z = \beta_z - j\alpha_z$. Here, we have applied the closed-form expression for k_z, modified from [14] as shown below:

$$k_z = \left\{ k_1^2 - \left(\frac{m\pi}{a}\right)^2 - \left(\frac{n\pi}{b}\right)^2 + 2(1-j)\frac{\delta\mu_1}{a\mu_2}\left[\left(\frac{m\pi}{a}\right)^2 + \left(\frac{n\pi}{b}\right)^2 + k_1^2\right] \right\}^{0.5}, \tag{3}$$

where k_1 is the wavenumber of the core material, μ_1 and μ_2 are respectively the permeability of the core and cladding materials; whereas m and n are respectively the number of half cycle variations in the x and y directions. The skin depth δ in (3) is given by [15]:

$$\delta = \frac{2Z_S}{(1+j)\omega\mu_2}, \tag{4}$$

where ω is the angular frequency. The surface impedance of the dielectric layer Z_S can be expressed in terms of the electrical properties of the two mediums as [7, 16]:

$$Z_S = \frac{1}{j\omega b(\varepsilon_{r1} - \varepsilon_{r2})}, \tag{5}$$

where ε_{rd} and ε_{r0} are respectively the relative permittivity of the core and the cladding materials. To account for the loss at the four corner regions, we employ the formulation developed by Deck et al. [13] by means of the perturbation theory. When deriving the correction to the mode propagation and profile function, correction to the dielectric function in the four corner regions is assumed to produce changes in the squared propagation constant and fields profile function [13]. The corner field correction factor $\Delta\Lambda$ can be expressed as [13]:

$$\Delta\Lambda = \mathrm{Im}\left| \left(\frac{\varepsilon_1 - \varepsilon_2}{2}\right)\left(\frac{\omega}{c\gamma}\right)^2 \times \left\{1 + \left[\cos(k_y b) + \left(\frac{\varepsilon_1}{\varepsilon_2}\right)\left(\frac{\gamma}{k_y}\right)\sin(k_y b)\right]^2\right\} \times \frac{(2\gamma b + 1)}{1 + \left[\cos(k_y b) + \left(\frac{\varepsilon_1}{\varepsilon_2}\right)\left(\frac{\gamma}{k_y}\right)\sin(k_y b)\right]^2} \right| \Lambda, \tag{6}$$

where ε_1 and ε_2 are respectively the permittivity of the core and its cladding material, $\gamma = \left(\frac{\omega}{c}\right)^2(\varepsilon_1 - \varepsilon_2) - k_y^2$ and k_y is the transverse wavenumber in the y direction. For simplicity, we apply the closed-form expression of k_y in [6] as shown in (7) below:

$$k_y = \frac{\pi}{b}\left(\frac{\pi n_1^2 b\sqrt{n_1^2 - n_2^2}}{\pi n_1^2 b\sqrt{n_1^2 - n_2^2} + n_2^2\lambda}\right). \tag{7}$$

The total bending loss Λ_T can therefore be determined by including the additional loss found in (6) with the loss in (2), i.e., $\Lambda_T = \Lambda + \Delta\Lambda$.

III. RESULTS AND DISCUSSION

We compute the loss in a 2.4 × 1.3 mm^2 silicon rectangular waveguide, with bending radius R = 1 mm. The conductivities of silicon and the surrounding medium are given as 4.33×10^{-4} S/m and 8.0×10^{-15} S/m, respectively. To validate the closed-form formulations presented here, we compare the computed results with the S21 parameters found from the Finite Element Method (FEM). The results from FEM are simulated from Ansoft's High Frequency Structure Simulator HFSS. Since S21 accounts for the total loss in the waveguide, we have incorporated the total dielectric loss α_z, i.e., the imaginary component of (3) together with the bending loss in (2) during comparison. When calculating the loss, we have set m = 1 and n = 0 for the dominant TE mode. It is worthwhile noting that, the loss in a practical waveguide may also be contributed from the imperfection of the waveguide structure. Since the work presented here is a theoretical exercise, such loss has therefore been neglected.

Figure 2 depicts the comparison of loss between our computed result and that obtained from HFSS. It can be seen from the figure that although the curves agree somewhat with each other, the loss from the computed result has clearly been underestimated. The average error with reference to the FEM result ε_{ave} = 60.17%. Since Marcuse has neglected the presence of the electric field in the x direction E_x, the loss of the E^x mode has not been taken into account. As shown in [6], the modes propagating in a dielectric waveguide are degenerate – both E^y and E^x modes exist concurrently and that the propagation constants of both modes are similar to each other. Figure 3 shows the total loss (i.e., the addition of dielectric and bending losses) when both E^x and E^y modes are taken into account. It can be observed from Fig. 4 that the electric fields of the E^x and E^y modes are orthogonal to each other. Despite their direction of polarizations, however, the profiles exhibited by both modes are qualitatively similar to each other [3]. Here, we have taken the bending loss exhibited by the E^x mode to be identical with that by E^y. The result turns out to be in closer agreement with that obtained from the FEM method, although discrepancy between the results is still apparent (ε_{ave} = 44.53%). Figure 5 shows the final result when the corner field correction factor $\Delta\Lambda$ has been included into our calculation. By considering the loss at the four edges of the waveguide, it can be observed from the figure that the result improves significantly, with the computed result approaches that of the simulation (ε_{ave} = 21.27%).

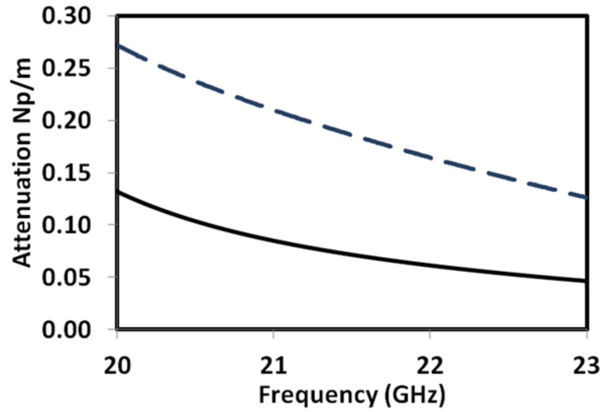

Fig. 2. Loss of a bent rectangular silicon waveguide, obtained from the analytical method proposed here (solid line) and the FEM (dashed line). The analytical method has only considered the dielectric loss and the bending loss from the E^y mode (loss at the corner regions has been neglected).

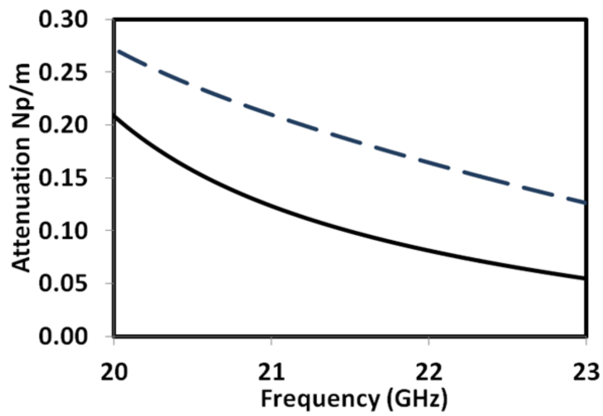

Fig. 3. Loss of a bent rectangular silicon waveguide, obtained from the analytical method proposed here (solid line) and the FEM (dashed line). The analytical method has only considered the dielectric loss and the bending loss from the E^y and E^x modes (loss at the corner regions has been neglected).

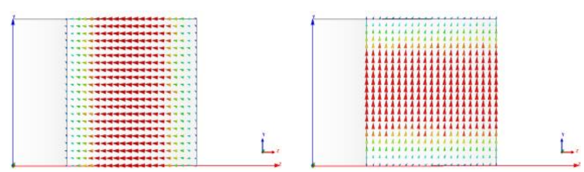

(a) (b)

Fig. 4. Electric field lines of: (a) E^x and (b) E^y modes at the cross section of the rectangular waveguide.

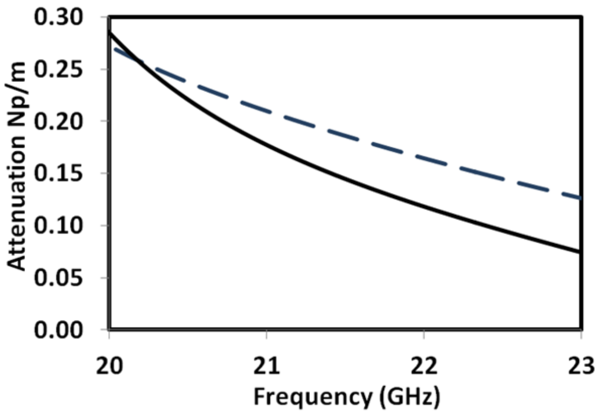

Fig. 5. Loss of a bent rectangular silicon waveguide, obtained from the analytical method proposed here (solid line) and the FEM (dashed line). The analytical method has taken into account the dielectric loss, as well as, the bending loss from the E^y and E^x modes (loss at the corner regions has been included).

IV. CONCLUSION

We have presented a closed-form analytical method to predict the attenuation in a bent dielectric rectangular waveguide. The dielectric loss in the waveguide can be extracted from the propagation constant obtained from a straight waveguide; whereas, the bending loss in the waveguide is determined from Marcuse' approximate method [12]. To enhance the accuracy of Marcuse' method, the correction factor in [13] has been applied to account for the loss at the corner regions. By including the bending loss exhibited by both E^y and E^x modes and the dielectric loss, the result is found to agree closely with that computed using the rigorous computational method. Since the formulations presented here are all in closed-form, it is not necessary to rely on computational intensive machines, such as a computer to calculate them. Besides being straight forward, the method also produces results which can be easily found; while at the same time, sufficiently accurate.

ACKNOWLEDGMENT

Part of this work has been supported by the FRGS Grant (Project: FRGS/2/2013/SG02/UTAR/02/1).

REFERENCES

[1] D. K. Cheng, *Field and Wave Electromagnetics*. 2nd ed., Addison Wesley Inc., 1989.

[2] R. E. Collin, *Field Theory of Guided Waves*. 2nd ed., IEEE Press, New York, 1991.

[3] E. A. J. Marcatili, "Bends in optical dielectric guides," *The Bell System Technical Journal*, vol. 48, no. 9, pp. 2103-2132, 1969.

[4] Y. Cai, T. Mizumoto, and Y. Naito, "Improved perturbation feedback method for the analysis of rectangular dielectric waveguides," *Journal of Lightwave Technology*, vol. 9, no. 10, pp. 1231-1237, 1991.

[5] P. R. Young and R. J. Collier, "Solution of lossy dielectric waveguides using dual effective-index method," *Electronics Letters*, vol. 33, no. 21, pp. 1788-1789, 1997.

[6] E. A. J. Marcatili, "Dielectric rectangular waveguide and directional coupler for integrated optics," *The Bell System Technical Journal*, vol. 48, no. 9, pp. 2071-2102, 1969.

[7] K. H. Yeap, K. H. Teh, K. C. Yeong, K. C. Lai, and M. C. Loh, "Propagation in dielectric rectangular waveguides," *Optica Applicata*, vol. 46, no. 2, pp. 317-330, 2016.

[8] D.-P. Cai, S.-C. Nien, H.-K. Chiu, C.-C. Chen, and C.-C. Lee, "Electrically tuneable liquid crystal waveguide attenuators," *Optics Express*, vol. 19, no. 12, pp. 11890-11896, 2011.

[9] H.-K. Chiu, F.-L. Hsiao, C.-H. Chan, and C.-C. Chen, "Compact and low-loss bent hollow waveguides with distributed Bragg reflector," *Optics Express*, vol. 16, no. 19, pp. 15069-15073, 2008.

[10] S.-S. Lo, C.-C. Chen, S.-C. Hsu, and C.-Y. Liu, "Fabricating a hollow optical waveguide for optical communication applications," *Journal of Microelectromechanical Systems*, vol. 15, no. 3, pp. 584-587, 2006.

[11] S.-S. Lo, M.-S. Wang, and C.-C. Chen, "Semiconductor hollow optical waveguides formed by omni-directional reflectors," *Optics Express*, vol. 22, no. 26, pp. 6589-6593, 2004.

[12] D. Marcuse, "Bending losses of the asymmetric slab waveguide," *The Bell System Technical Journal*, vol. 50, no. 8, pp. 2551-2563, 1971.

[13] R. T. Deck, M. Mirkov, and B. G. Bagley, "Determination of bending losses in rectangular waveguides," *Journal of Lightwave Technology*, vol. 16, no. 9, pp. 1703-1714, 1998.

[14] P. I. Somlo and J. D. Hunter, "On the TE10 mode cutoff frequency in lossy-walled rectangular waveguides," *IEEE Transactions on Instrumentation and Measurement*, vol. 45, pp. 301-304, 1996.

[15] T. K. Hong, "Analysis of Loss in Dielectric Waveguides," *Universiti Tunku Abdul Rahman*, Malaysia, B.Eng., 2014.

[16] B. M. Kolundžija and A. R. Djordjević, *Field Integral Equations*. In: Electromagnetic Modeling of Composite Metallic and Dielectric Structure, Artech House, Massachusetts, pp. 181-182, 2002.

Ultra-Wide Bandwidth Enhancement of Single-Layer Single-Feed Patch Antenna Using the Theory of Characteristic Modes

Mohamed M. Elsewe and Deb Chatterjee

Computer Science & Electrical Engineering Department
University of Missouri – Kansas City, Kansas City, MO 64110, USA
mme0f0@mail.umkc.edu, chatd@umkc.edu

Abstract **─** The Theory of Characteristic Modes (TCM) is proposed as a systematic approach to antenna design to achieve the goal of finding the antenna structure with optimum broadband behavior. This theory provides a physical insight to the radiating nature of microstrip patch antennas and reduces the design optimization time. In this work, the resonant behavior of the highly radiating structure of the single U-slot rectangular patch on a single-layer ε_r = 4.4 substrate is analyzed using TCM. Modal analysis of this single-layer structure with different single feed excitations concludes that VSWR ≤ 2 impedance bandwidth in the order of 96% can be achieved with a single T-probe feed. Experimental results, included here, show VSWR ≤ 2 impedance bandwidth in the order of 71%.

Index Terms **─** Bandwidth broadening, characteristic mode analysis, L-probe, microstrip patch antennas, T-probe, theory of characteristic modes, U-slot, UWB.

I. INTRODUCTION

The need for antennas with high bandwidth is continuing to fuel a lot of research especially in the fields of radar, wireless communication and medical imaging. Microstrip patch antennas are a class of antennas that exhibit low-profile, compact, conformal, cost-effective, and easy-to-fabricate designs. Despite these advantages, microstrip patch antennas suffer from a major drawback, which is narrow bandwidth. For the past couple of decades, extensive research has been dedicated to the area of bandwidth broadening techniques of microstrip patch antennas. Some of these techniques are by means of introduction of parasitic elements and patch slots, which introduce additional resonances in addition to the main patch resonance. Another technique is by means of thick substrates of low permittivity, which will have the side effect of introducing higher inductive reactance due to the longer coaxial feed probe. Some of the patch slot geometries found in the literature are: square, rectangular, triangular, circular, elliptical, E-slot, U-slot, V-slot, and more [1, 2]. Although it is generally understood that patch slots introduce new resonances that contribute to broadening the bandwidth, it is not well understood why some patch slots present better bandwidth than others. A valuable tool that is helping antenna designer's gain better understanding and physical insight of the radiating nature and resonant behavior of the microstrip patch antenna is the TCM [3, 4]. By understanding the resonant behavior of the different patch slot geometries and other antenna elements, novel antenna designs with the most resonant structures can be proposed to achieve the most radiation and impedance bandwidth.

In recent studies [5-7], we utilized TCM to characterize the resonant behavior of different patch slot geometries, substrate permittivities and ground sizes independent of the feeding element to identify the structures which are more resonant, and hence, contribute significantly to the radiated fields. It was concluded that a single U-slot rectangular patch on a single-layer substrate with relative permittivity of 4.4 and loss tangent of 0.02 will result in a highly radiating structure.

It is the aim of this paper to expand on these recent studies [5-8] and to find the ideal excitation feed to excite the highly radiating structure of the U-slot rectangular patch on ε_r = 4.4 substrate to achieve the most radiation and impedance bandwidth. TCM will be utilized once more to analyze some of the different excitation feeds found in the literature [9] to determine the least reactive excitation feed structure, which will excite the modes contributing to the optimum resonant behavior of the U-slot patch antenna.

II. MODAL ANALYSIS OF EXCITATION FEEDS FOR U-SLOT PATCH ANTENNA

Modal significance is defined as the normalized amplitude of the characteristic modes. Modes where the modal significance is close to 1 indicate that they contribute significantly to radiation, whereas modes with modal significance close to 0 indicate they do not [4]. Therefore, modal significance gives the antenna designer physical insight on the resonant behavior of an antenna structure independent of the source excitation.

Submitted On: October 20, 2016
Accepted On: November 15, 2016

Before we model the highly radiating structure of U-slot patch and ε_r = 4.4 substrate with an excitation feed, we need to first investigate which eigenmodes are resonating on this structure. In Fig. 1, the modal significance of the top 6 significant eigenmodes is shown. It is shown that modes 1, 3, and 4 contribute the most to radiation since their modal significance is close to 1 over the frequency range 2.5-8.5 GHz. Higher order modes 5 and 6 contribute minimally in the higher frequencies. So, prospective excitation sources will aim to excite all or some of the resonating eigenmodes (1, 3, and 4) in the antenna structure.

Figure 2 shows the characteristic currents for modes 1, 3, and 4 at 5.0 GHz. The location of maximum current distribution, where it is desirable to excite the patch, is denoted by the concentrated red color in Fig. 2. The common location for maximum current distribution between all three modes is marked by the dotted black circles in Fig. 2 and is found to be at the base of the U-slot and the inner edge of the U-slot arm.

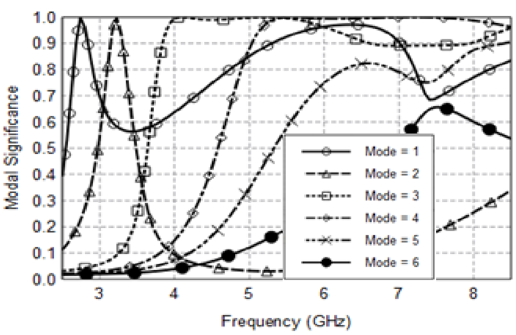

Fig. 1. Modal significance for U-slot patch antenna with ε_r = 4.4 substrate.

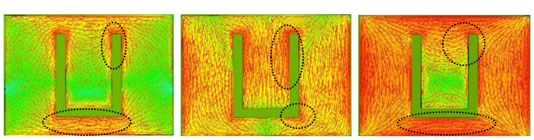

(a) (b) (c)

Fig. 2. Characteristic currents of U-slot rectangular patch antenna on ε_r = 4.4 substrate at 5.0 GHz for: (a) mode 1, (b) mode 3, and (c) mode 4.

To find an ideal source feed which will excite the most modes, modal analysis of the U-slot rectangular patch antenna on the ε_r = 4.4 substrate with tan(δ) = 0.02 is performed with 3 different probe feeds, namely the conventional vertical probe, the L-probe, and the T-probe, shown in Fig. 3. The U-slot patch antenna and probe dimensions, designed using the method of dimensional invariance [1] for a 3.9 GHz design frequency, are shown in the first three columns in Table 1 for each of the probes. The probe radius is defined as r_p. The x- and y-axis positions of the probe are defined as x_p and y_p, respectively. The probes are placed at the location of maximum current distribution marked in Fig. 2. The horizontal and vertical arms of the L-probe and T-probe are defined as L_h and L_v, respectively. The horizontal arm of the T-probe is symmetric, i.e., its length on the left side of vertical arm is equal to its length on the right side of vertical arm, which is equal to 3.84 mm.

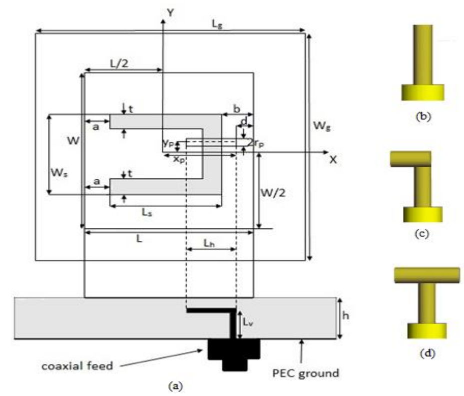

Fig. 3. (a) Geometry of rectangular patch antenna with U-slot, (b) vertical probe, (c) L-probe, and (d) T-probe.

Table 1: U-slot patch antenna dimensions in mm for different feed probe designs

	Vertical Probe (Sim.)	L-Probe (Sim.)	T-Probe (Sim.)	T-Probe (Fabricated)
a	2.25	2.25	2.25	4.38
b	2.25	2.25	2.25	4.38
W	20.25	20.25	20.25	39.48
L	14.62	14.62	14.62	28.51
L_s	10.14	10.14	10.14	19.78
t	1.13	1.13	1.13	2.21
W_s	7.87	7.87	7.87	15.35
W_g	140.17	140.17	140.17	139.41
L_g	134.54	134.54	134.54	128.44
h	7.62	7.62	7.62	15.35
r_p	1	1	1	0.65
x_p	6	4.81	4	10.95
y_p	5	1	1	0
L_h	----	3.84	3.84	2.99x2.28
L_v	7.62	6.53	6.15	12.80
d	1.31	2.5	3.31	3.31

In [8], we performed a modal excitation analysis over the selected frequency range 2.5-8.5 GHz on the U-slot rectangular patch slot and ε_r = 4.4 substrate with vertical probe, L-probe, and T-probe to determine which source feed excites the modes 1, 3, and 4, which contribute to the optimum resonant behavior. It was found that mode 3 is the main mode excited by the conventional vertical probe in the frequency range 2.5-5.7 GHz. Mode 3 is the main mode excited by the

L-probe in the frequency range 2.5-6.1 GHz. Modes 3, 4, and 6 are the main modes excited by the T-probe in the frequency range 2.5-7.0 GHz. Consequently, the T-probe excites the most number of modes over the largest frequency range, and hence, is expected to achieve the highest impedance bandwidth.

In Fig. 4, the modal significance of each of the three probes is shown. The non-excited probe structures are modeled independent of the other antenna elements, i.e., the U-slot patch, substrate, and ground plane. For the vertical probe, in Fig. 4 (a), mode 1 is the contributing mode maxing out at modal significance equal to 0.08. For the L-probe, in Fig. 4 (b), mode 1 is the contributing mode maxing out at modal significance close to 0.16. For the T-probe, in Fig. 4 (c), modes 1 and 2 are the contributing modes maxing out at modal significance close to 0.20. Compared to the other two probes, the T-probe has more modes with higher modal significance which indicates that it is the least reactive feeding structure. This is a desirable feeding structure feature and also explains why the T-probe is expected to achieve the highest impedance bandwidth. The fact that the modal significance of all the probes is relatively low at less than 0.20 indicates that they will not contribute much to the radiation of the entire antenna, which is another desirable feature in feeding structures.

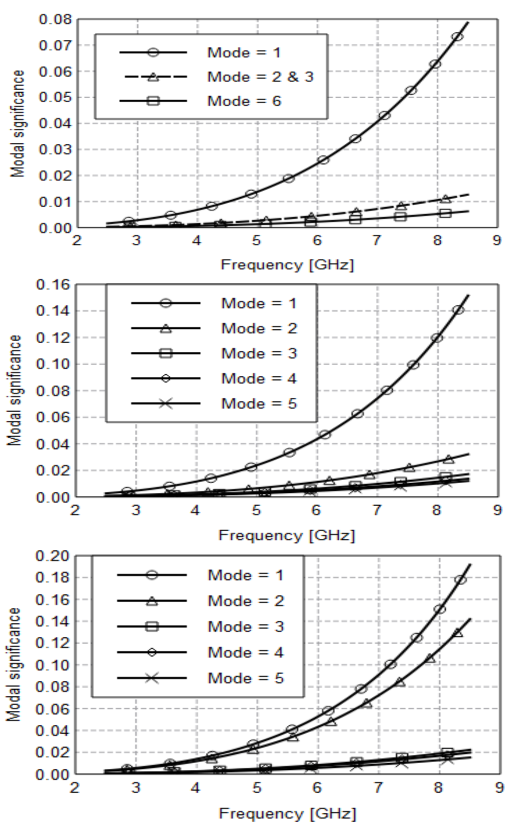

Fig. 4. Modal significance of different excitation feeds: (a) vertical probe, (b) L-probe, and (c) T-probe.

III. OPTIMIZED IMPEDANCE BANDWIDTH OF U-SLOT PATCH ANTENNA

Figure 5 shows the VSWR ≤ 2 bandwidth for the 3.9 GHz U-slot patch design with 3 different probes (dimensions shown in the first three columns of Table 1). Results from two electromagnetic solvers, namely FEKO FEM and HFSS FEM, are shown for validation purposes. The vertical probe in Fig. 5 (a) shows VSWR ≤ 2 bandwidth of 21% between 3.55 GHz and 4.38 GHz. The L-probe feed in Fig. 5 (b) shows VSWR ≤ 2 bandwidth of 82% between 2.74 GHz and 6.58 GHz, and the T-probe feed in Fig. 5 (c) shows VSWR ≤ 2 bandwidth of 96% between 2.86 GHz and 8.16 GHz. The simulation results of the two solvers are in good agreement.

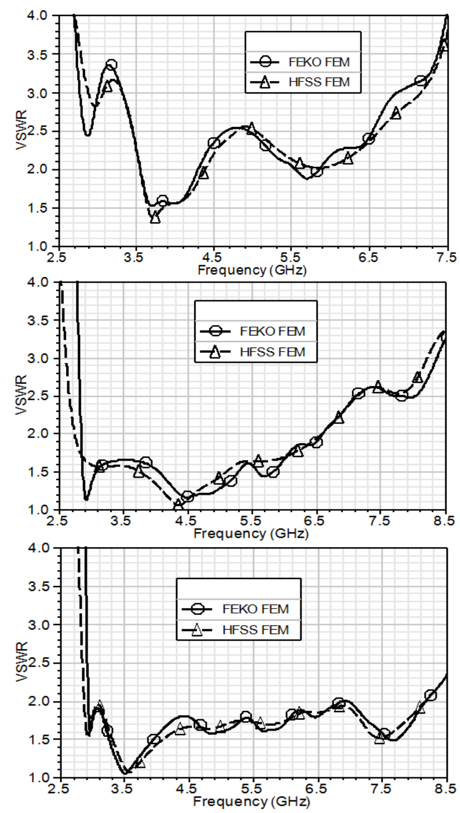

Fig. 5. Simulated VSWR for U-slot patch antenna with different excitation feeds: (a) vertical probe, (b) L-probe, and (c) T-probe.

The small substrate thickness of 7.62 mm used in the T-probe fed antenna design simulation of Fig. 5 (c) was not available for fabrication. Also, the horizontal probe arm of the T-probe was modeled as a rectangular PEC sheet sandwiched between two substrate layers due to lack of proper instrumentation to fabricate a T-shaped probe. Therefore, a bigger patch antenna with thicker multilayered substrate was fabricated for a 2.0 GHz design frequency, instead. The dimensions of the fabricated T-probe fed U-slot patch antenna are shown in the rightmost fourth column of Table 1. Figure 6 shows the measured and simulated VSWR ≤ 2 bandwidth of the fabricated antenna. As seen in Fig. 6, measured VSWR ≤ 2 bandwidth of over 71% between 1.8 GHz and 3.8 GHz is realized, though bandwidth can be improved between 2.2 and 2.4 GHz. Also, a higher VSWR ≤ 2 bandwidth between 1.8 and 4.8 GHz could be realized if it was not for the oscillations around 2.3, 3.9, and 4.5 GHz. These oscillations are mainly due to the thicker substrate used in fabrication which introduces more surface waves that scatter at substrate edges. The slight discrepancy between the measured and simulated results in Fig. 6 can be attributed to fabrication inaccuracies and manufacturing tolerances, otherwise the pattern demonstrated by the two curves mostly agree.

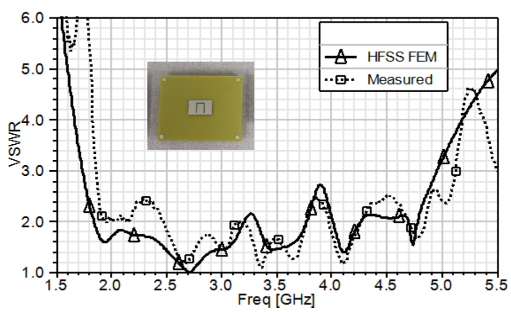

Fig. 6. Measured vs simulated VSWR of fabricated T-probe fed, U-slot microstrip patch antenna with $\varepsilon_r = 4.4$ substrate. Inset: image of fabricated antenna.

IV. CONCLUSION

In this paper, the Theory of Characteristic Modes has been used to find the ideal excitation feed to excite the highly radiating structure of the U-slot rectangular patch on $\varepsilon_r = 4.4$ substrate to achieve the most radiation and impedance bandwidth. Different excitation feeds, namely the vertical probe, L-probe, and T-probe were analyzed to determine the least reactive excitation feed structure, which will excite the modes contributing to the optimum resonant behavior of the U-slot patch antenna. Simulated and experimental results show that a single T-probe feed excites the most number of modes and achieves impedance bandwidth in excess of 70%.

REFERENCES

[1] V. Natarajan and D. Chatterjee, “Comparative evaluation of some empirical design techniques for CAD optimization of wideband U-Slot microstrip antennas,” *Applied Computational Electromagnetics Society (ACES) Journal*, vol. 20, no. 1, pp. 50-69, March 2005.

[2] G. Rafi, and L. Shafai, “Broadband microstrip patch antenna with V-slot,” *IEE Proceedings Microwaves Antennas and Propagation*, vol. 151, no. 5, pp. 435-440, 2004.

[3] R. F. Harrington and J. R. Mautz, “Theory of characteristic modes for conducting bodies,” *IEEE Trans. Antennas Propag.*, vol. AP-19, no. 5, pp. 622–628, Sept. 1971.

[4] M. Vogel, G. Gampala, D. Ludick, U. Jakobus, and C.J. Reddy, “Characteristic mode analysis: putting physics back into simulation,” *IEEE Antennas Propag. Mag.*, vol. 57, no. 2, pp. 307-317, Apr. 2015.

[5] M. M. Elsewe and D. Chatterjee, “Modal analysis of patch slot designs in microstrip patch antennas,” *2016 IEEE International Conference on Wireless Information Technology and Systems (ICWITS) and Applied Computational Electromagnetics (ACES)*, Honolulu, HI, March 13-17, 2016.

[6] M. M. Elsewe and D. Chatterjee, “Modal analysis of substrate permittivities in microstrip patch antennas,” *2016 IEEE International Conference on Wireless Information Technology and Systems (ICWITS) and Applied Computational Electromagnetics (ACES)*, Honolulu, HI, March 13-17, 2016.

[7] M. M. Elsewe and D. Chatterjee, "Characteristic mode analysis of ground plane size in microstrip patch antennas," *2016 IEEE International Symposium on Antennas and Propagation & USNC/URSI National Radio Science Meeting*, Fajardo, Puerto Rico, June 26-July 1, 2016.

[8] M. M. Elsewe and D. Chatterjee, "Characteristic mode analysis of excitation feed probes in microstrip patch antennas," *2016 IEEE International Symposium on Antennas and Propagation & USNC/URSI National Radio Science Meeting*, Fajardo, Puerto Rico, June 26-July 1, 2016.

[9] C.L. Mak, K.F. Lee, and K.M. Luk, “Broadband patch antenna with a T-shaped probe,” *IEE Proceedings Microwaves Antennas and Propagation*, vol. 147, no. 2, pp. 73-76, 2000.

APPLIED COMPUTATIONAL ELECTROMAGNETICS SOCIETY EXPRESS JOURNAL
http://aces-society.org

INFORMATION FOR AUTHORS

PUBLICATION CRITERIA

Each paper is required to manifest some relation to applied computational electromagnetics. **Papers may address general issues in applied computational electromagnetics, or they may focus on specific applications, techniques, codes, or computational issues.** While the following list is not exhaustive, each paper will generally relate to at least one of these areas:

1. **Code validation.** This is done using internal checks or experimental, analytical or other computational data. Measured data of potential utility to code validation efforts will also be considered for publication.

2. **Code performance analysis.** This usually involves identification of numerical accuracy or other limitations, solution convergence, numerical and physical modeling error, and parameter tradeoffs. However, it is also permissible to address issues such as ease-of-use, set-up time, run time, special outputs, or other special features.

3. **Computational studies of basic physics.** This involves using a code, algorithm, or computational technique to simulate reality in such a way that better, or new physical insight or understanding, is achieved.

4. **New computational techniques** or new applications for existing computational techniques or codes.

5. **"Tricks of the trade"** in selecting and applying codes and techniques.

6. **New codes, algorithms, code enhancement, and code fixes.** This category is self-explanatory, but includes significant changes to existing codes, such as applicability extensions, algorithm optimization, problem correction, limitation removal, or other performance improvement. **Note: Code (or algorithm) capability descriptions are not acceptable, unless they contain sufficient technical material to justify consideration.**

7. **Code input/output issues.** This normally involves innovations in input (such as input geometry standardization, automatic mesh generation, or computer-aided design) or in output (whether it be tabular, graphical, statistical, Fourier-transformed, or otherwise signal-processed). Material dealing with input/output database management, output interpretation, or other input/output issues will also be considered for publication.

8. **Computer hardware issues.** This is the category for analysis of hardware capabilities and limitations of various types of electromagnetics computational requirements. Vector and parallel computational techniques and implementation are of particular interest.

Applications of interest include, but are not limited to, antennas (and their electromagnetic environments), networks, static fields, radar cross section, inverse scattering, shielding, radiation hazards, biological effects, biomedical applications, electromagnetic pulse (EMP), electromagnetic interference (EMI), electromagnetic compatibility (EMC), power transmission, charge transport, dielectric, magnetic and nonlinear materials, microwave components, MEMS, RFID, and MMIC technologies, remote sensing and geometrical and physical optics, radar and communications systems, sensors, fiber optics, plasmas, particle accelerators, generators and motors, electromagnetic wave propagation, non-destructive evaluation, eddy currents, and inverse scattering.

Techniques of interest include but not limited to frequency-domain and time-domain techniques, integral equation and differential equation techniques, diffraction theories, physical and geometrical optics, method of moments, finite differences and finite element techniques, transmission line method, modal expansions, perturbation methods, and hybrid methods.

Where possible and appropriate, authors are required to provide statements of quantitative accuracy for measured and/or computed data. This issue is discussed in "Accuracy & Publication: Requiring, quantitative accuracy statements to accompany data," by E. K. Miller, ACES Newsletter, Vol. 9, No. 3, pp. 23-29, 1994, ISBN 1056-9170.

SUBMITTAL PROCEDURE

All submissions should be uploaded to ACES server through ACES web site (http://aces-society.org) by using the upload button, Express Journal section. Only pdf files are accepted for submission. The file size should not be larger than 6MB, otherwise permission from the Editor-in-Chief should be obtained first. Automated acknowledgment of the electronic submission, after the upload process is successfully completed, will be sent to the corresponding author only. It is the responsibility of the corresponding author to keep the remaining authors, if applicable, informed. Email submission is not accepted and will not be processed.

EDITORIAL REVIEW

In order to ensure an appropriate level of quality control, papers are peer reviewed. They are reviewed both for technical correctness and for adherence to the listed guidelines regarding information content and format.

PAPER FORMAT

Only camera-ready electronic files are accepted for publication. The term **"camera-ready" means that the material is neat, legible, reproducible, and in accordance with the final version format listed below.**

The following requirements are in effect for the final version of an ACES Express Journal paper:

1. The paper title should not be placed on a separate page. The title, author(s), abstract, and (space permitting) beginning of the paper itself should all be on the first page. The title, author(s), and author affiliations should be centered (center-justified) on the first page. The title should be of font size 14 and bolded, the author names should be of font size 12 and bolded, and the author affiliation should be of font size 10 (regular font, neither italic nor bolded).

2. An abstract is required. The abstract should be a brief summary of the work described in the paper. It should state the computer codes, computational techniques, and applications discussed in the paper (as applicable) and should otherwise be usable by technical abstracting and indexing services. The word "Abstract" has to be placed at the left margin of the paper, and should be bolded and italic. It also should be followed by a hyphen (–) with the main text of the abstract starting on the same line.

3. All section titles have to be centered and all the title letters should be written in caps. The section titles need to be numbered using roman numbering (I. II. ….)

4. Either British English or American English spellings may be used, provided that each word is spelled consistently throughout the paper.

5. Internal consistency of references format should be maintained. As a guideline for authors, we recommend that references be given using numerical numbering in the body of the paper (with numerical listing of all references at the end of the paper). The first letter of the authors' first name should be listed followed by a period, which in turn, followed by the authors' complete last name. Use a comma (,) to separate between the authors' names. Titles of papers or articles should be in quotation marks (" "), followed by the title of the journal, which should be in italic font. The journal volume (vol.), issue number (no.), page numbering (pp.), month and year of publication should come after the journal title in the sequence listed here.

6. Internal consistency shall also be maintained for other elements of style, such as equation numbering. Equation numbers should be placed in parentheses at the right column margin. All symbols in any equation have to be defined before the equation appears or right immediately following the equation.

7. The use of SI units is strongly encouraged. English units may be used as secondary units (in parentheses).

8. Figures and tables should be formatted appropriately (centered within the column, side-by-side, etc.) on the page such that the presented data appears close to and after it is being referenced in the text. When including figures and tables, all care should be taken so that they will appear appropriately when printed in black and white. For better visibility of paper on computer screen, it is good to make color figures with different line styles for figures with multiple curves. Color should also be tested to insure their ability to be distinguished after black and white printing. Avoid the use of large symbols with curves in a figure. It is always better to use different line styles such as solid, dotted, dashed, etc.

9. A figure caption should be located directly beneath the corresponding figure, and should be fully justified.

10. The intent and meaning of all text should be clear. For authors who are not masters of the English language, the ACES Editorial Staff will provide assistance with grammar (subject to clarity of intent and meaning). However, this may delay the scheduled publication date.

11. Unused space should be minimized. Sections and subsections should not normally begin on a new page.

ACES reserves the right to edit any uploaded material, however, this is not generally done. It is the author(s) responsibility to provide acceptable camera-ready files in pdf and MSWord formats. Incompatible or incomplete files will not be processed for publication, and authors will be requested to re-upload a revised acceptable version.

COPYRIGHTS AND RELEASES

Each primary author must execute the online copyright form and obtain a release from his/her organization vesting the copyright with ACES. Both the author(s) and affiliated organization(s) are allowed to use the copyrighted material freely for their own private purposes.

Permission is granted to quote short passages and reproduce figures and tables from an ACES Express Journal issue provided the source is cited. Copies of ACES Express Journal articles may be made in accordance with usage permitted by Sections 107 or 108 of the U.S. Copyright Law. The consent does not extend to other kinds of copying, such as for general distribution, for advertising or promotional purposes, for creating new collective works, or for resale. The reproduction of multiple copies and the use of articles or extracts for commercial purposes require the consent of the author and specific permission from ACES. Institutional members are allowed to copy any ACES Express Journal issue for their internal distribution only.

PUBLICATION CHARGES

There is a $200 basic publication charge assigned to each paper for ACES members, and $300 charge for non-ACES members. Corresponding authors should be active members of the society at the time of submission and the time of publication in order to receive the reduced charge.

ACES Express Journal doesn't allow for more than four pages. All authors must comply with the page limitations. ACES Express Journal is an online journal, and printed copies are not available.

Upon completion of its first year, ACES Express Journal will be abstracted in INSPEC, in Engineering Index, DTIC, Science Citation Index Expanded, the Research Alert, and to Current Contents/Engineering, Computing & Technology.